Acta Cryst. (1993). B49, 579–591

The Incommensurately Modulated Structures of the Blue Bronzes $K_{0.3}MoO_3$ and $Rb_{0.3}MoO_3$

BY W. J. SCHUTTE AND J. L. DE BOER

Materials Science Centre, Laboratory of Inorganic Chemistry, University of Groningen, Nijenborgh 16, 9747 *AG Groningen, The Netherlands*

(*Received* 24 *October* 1990; *accepted* 19 *June* 1992)

Abstract

The incommensurately modulated structures of the isostructural blue bronzes of K and Rb with modulation wavevector $\mathbf{q} = \mathbf{a}^* + 0.748\,(1)\mathbf{b}^* + \frac{1}{2}\mathbf{c}^*$ at 100 K have been determined by X-ray diffraction. The lattice parameters of the *C*-centred monoclinic cell for $K_{0.3}MoO_3$ are: $a = 18.162\,(2)$, $b = 7.554\,(1)$, $c = 9.816\,(1)$ Å, $\beta = 117.393\,(6)°$, $V = 1195.7$ Å^3, $Z = 20$, $\mu = 55.7$ cm^{-1}, $\lambda = 0.7107$ Å, $M_r = 156.9$. For $Rb_{0.3}MoO_3$: $a = 18.536\,(2)$, $b = 7.556\,(1)$, $c = 10.035\,(5)$ Å, $\beta = 118.52\,(1)°$, $V = 1234.9$ Å^3, $Z = 20$, $\mu = 110.0$ cm^{-1}, $\lambda = 0.7107$ Å, $M_r = 172.4$. The symmetry of the structure can be described as consisting of a one-dimensionally modulated system with the four-dimensional superspace group $C_s^{C2/m}(0\beta\frac{1}{2})$. The final $R_F = 0.033$ for 7985 reflections for the K bronze and 0.032 for 4458 reflections for the Rb bronze. In the modulated structure, valence calculations show that the phase transition to the semiconductor state is accompanied by ordering of Mo^{5+} along the infinite-chain direction. The metallic conductivity, with delocalization of 4*d* electrons between clusters by overlapping Mo–O–Mo orbitals along the infinite-chain direction, turns into semiconductor properties by localization of 4*d* electrons on individual Mo(2) and Mo(3) octahedra (not on $Mo_{10}O_{30}$ clusters as a whole), modulated with wavevector **q**. By a comparison of the structures of the blue and red bronzes, their physical properties can be interpreted.

1. Introduction

The blue bronzes belong to the series of compounds A_xTO_n in which A is an alkali metal and T a transition metal. Most blue bronzes were synthesized for the first time about 25 years ago, but only in recent years have their low-dimensional and associated charge-density-wave (CDW) properties been recognized (reviewed by, for example, Schlenker & Dumas, 1986; Schlenker, 1989).

While the W bronzes with delocalized 5*d* electrons have a large conductivity and the V bronzes with localized 3*d* electrons are nonmetallic (Goodenough, 1970), the Mo bronzes with 4*d* electrons are intermediate and often show a metal-to-semiconductor (or metal-to-metal) transition. Blue bronzes $A_{0.30}MoO_3$ are quasi-one-dimensional conductors and undergo a CDW transition, purple bronzes AMo_6O_{17} ($A_{0.15}MoO_{2.83}$) are quasi-two-dimensional conductors also having a CDW transition and the red bronzes $A_{0.33}MoO_3$ are semiconductors.

The existence of a metal-to-semiconductor transition in the blue bronzes at $T_c \simeq 180$ K has been studied extensively (reviewed by, for example, Hutiray & Solyom, 1985; Grüner, 1988). Electrical, magnetic and optical properties are strongly anisotropic and quasi-one-dimensional. The temperature variation of the conductivity is also anisotropic and in the semiconducting state ($T < 180$ K) it shows nonlinear behaviour due to sliding of the CDW (Dumas, Schlenker, Marcus & Buder, 1983).

The average crystal structure of the K blue bronze as determined by Graham & Wadsley (1966) is monoclinic, space group *C*2/*m*, with 20 formulae units in a unit cell. The structure contains rigid units composed of ten distorted MoO_6 octahedra, sharing their edges or corners to form a cluster. These clusters are linked together *via* corner sharing along and perpendicular to **b** and form slabs, held together by K atoms between them (see Fig. 1). The linking between cluster units is made by Mo(2) and Mo(3) octahedra, while the Mo(1) octahedron shares its edges and corners only with the Mo(2) and Mo(3) octahedra of the same unit. With such an arrangement $K_{0.3}MoO_3$ has been considered to be a two-dimensional layered compound as far as the MoO_3 sublattice is concerned.

At room temperature Weissenberg photographs showed diffuse streaks incommensurate with the crystal lattice (Pouget, Noguera, Moudden & Moret, 1985). Below 180 K these streaks condense into well defined satellite reflections with modulation wavevector $\mathbf{q} = q_y\mathbf{b}^* + \frac{1}{2}\mathbf{c}^*$ and q_y slightly greater than 0.25. Thus the transition at 180 K is a Peierls transition leading to an incommensurate semiconducting charge-density-wave state. In the following we take

the alternative choice for the modulation wavevector with q_y slightly less than 0.75.

Structural refinements of the average structure of the blue K and Rb bronzes at room temperature were carried out by Ghedira, Chenavas, Marezio & Marcus (1985) (in an *I*-centred unit cell). According to Ghedira *et al.* (1985), the data show that more than 80% of the 4*d* electrons are on Mo sites involved in the infinite chains. A model of the modulation of the Mo atoms at low temperature was given by Sato, Fujishita, Sato & Hoshino (1985). Recently, in a diffraction study (Colaitis, 1989), the satellite spots were interpreted, based on the concept of partial ordering from a nonstoichiometric phase. A model was proposed in which the ordering process is related to the occupation modulation of the alkali atoms. In our X-ray structure refinement we do not find any occupational modulation of the alkali atoms. All alkali sites are found to be fully occupied both above and below T_c. The different interpretation of the modulation in the diffraction study of Colaitis (1989) can probably be ascribed to inaccurate diffraction intensities. Since the diffraction data are not precise it is very difficult to find the displacive modulation amplitudes, in particular those of the less-heavy atoms.

To obtain a good insight into the structural modulations involved in the transition to the semiconducting state, we determined the complete modulated structure of the blue bronzes of K and Rb and analysed the structural distortions. We carried out a structure determination of the K blue bronze at 192 K (just above T_c) and compared the crystal structures of the closely related blue and red bronzes. Because no accurate crystal structures of the red bronzes have been published, we recalculated the structure of two red bronzes (Fig. 2), '$K_{0.26}MoO_3$' (Stephenson & Wadsley, 1965) and '$Cs_{0.25}MoO_3$' (Mumme & Watts, 1970).

2. Experimental

All diffraction experiments were performed with monochromatized Mo $K\alpha$ radiation on an Enraf–Nonius CAD-4F diffractometer equipped with a modified *CAD*-4 program (de Boer & Duisenberg, 1984). All observed reflections at 100 K could be indexed as *hklm* with *hkl* the Miller indices corresponding to the monoclinic subcell and $|m|$ the order of the satellite reflections of the modulation wavevector **q**. From a small single crystal of $K_{0.3}MoO_3$ (0.15 × 0.1 × 0.1 mm) the main reflections at 192 and 100 K were measured and from a larger single crystal (0.1 × 0.3 × 0.3 mm) the satellite reflections at 100 K were measured. We used two different crystals because of the weakness of the satellite reflections and to avoid secondary-extinction effects. The extra scaling factor for the data sets from the two crystals was derived by measuring for *h*,*k*,*l* with $k = 3,4$ not only the main reflections of the larger crystal but also some satellite reflections of the small crystal. A similar data set collection was done for $Rb_{0.30}MoO_3$ (small crystal: 0.02 × 0.2 × 0.1 mm; large crystal: 0.1 × 0.3 × 0.2 mm) at 100 K.

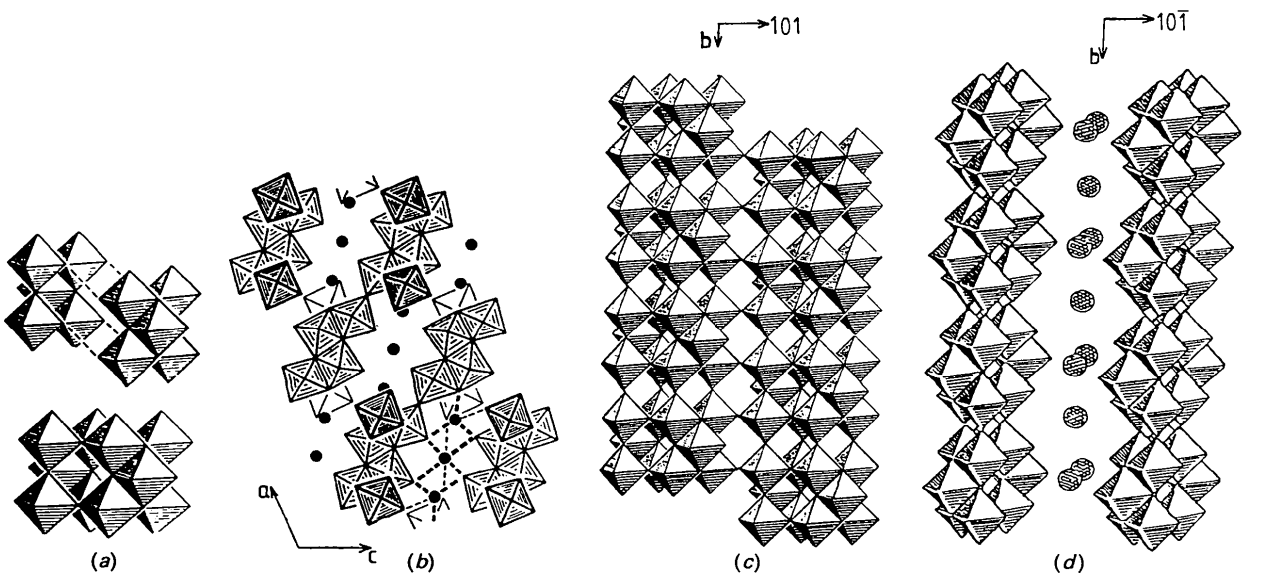

Fig. 1. Schematic diagrams for the basic structure of the blue bronze, described in the right-handed Graham & Wadsley (1966) cell with doubled *c* axis. (*a*) $Mo_{10}O_{30}$ cluster. (*b*) View along [0$\bar{1}$0], showing the upper view of octahedral slabs. The oxygen octahedra are outlined. (*c*) View along [10$\bar{1}$], four unit cells along **b** are drawn. (*d*) Perspective view along [101], four unit cells along **b**, infinite sheets of $Mo_{10}O_{30}$ clusters are seen.

Lattice parameters were obtained from the positions of 25 higher-order main reflections and the wavevector **q** was determined from accurately determined positions of first-order satellites. Cell constants and modulation wavevectors **q** for the blue bronzes are given in Table 1. For the $I(hklm)$ intensity measurements, the crystal was always placed in such a position as to minimize absorption effects. Intensity data were collected using the θ–2θ scan. Only first-order satellites could be measured; higher-order satellites were not observed. In view of the low intensities, satellite reflections were measured with lower scan speeds, in the ratio 5:2:1 for $|m| = 0,1$ for even k only and 1 for odd k only, respectively. Each data collection was split into subsets of constant m and the measurement of each of these subsets, defined in a unique sector of reciprocal space, was followed (except for the case of odd k satellites for the K bronze) by measurement of the equivalent sector obtained by rotation around the twofold axis. Throughout these subset measurements, three intensity-control reflections were monitored every 2 h and used for slight (within ±1.5%) drift corrections. In this way we obtained a data file for the K bronze at 192 K of 13 164 reflections ($\theta_{max} = 50°$). For the K bronze at 100 K we obtained, with the scaling reflections omitted, a data file of 13 116 main reflections ($\theta_{max} = 50°$) and 6688 satellite reflections ($\theta_{max} = 34°$). For the Rb bronze at 100 K we obtained a data file of 7986 main reflections ($\theta_{max} = 40°$) and 12 677 satellite reflections ($\theta_{max} = 40°$). Hereafter the data were corrected for Lorentz and polarization effects and for absorption (K bronze: $\mu^{K\ bronze} = 55.7\ cm^{-1}$; transmission factors: 0.29–0.68 for the large crystal, 0.55–0.65 for the small crystal; Rb bronze: $\mu^{Rb\ bronze} = 110.0\ cm^{-1}$; transmission factors: 0.17–0.47 for the large crystal, 0.32–0.79 for the small crystal) and unique data sets were subsequently obtained by averaging equivalent reflections; for details see Table 2.

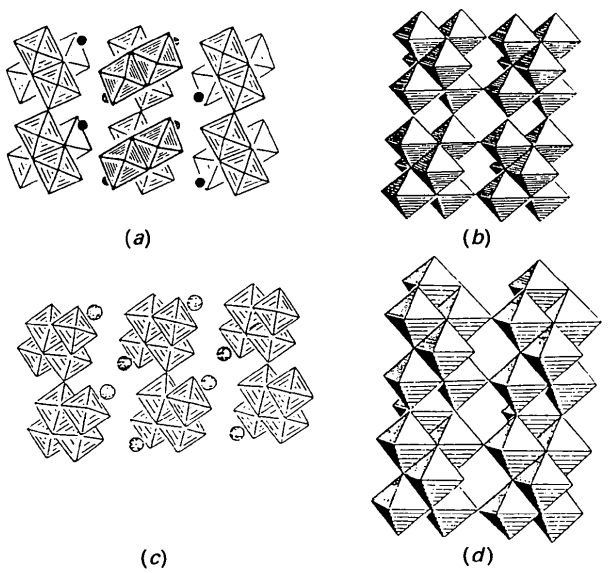

Fig. 2. Schematic diagrams of the structure of the red bronzes. (*a*), (*b*) *C*2/*m* structure (for '$K_{0.26}MoO_3$' and $Cs_{0.33}MoO_3$); (*c*), (*d*) $P2_1/m$ structure (for $Cs_{0.25}MoO_3$). (*a*), (*c*) Projection on [010] showing the upper view of the octahedral slabs. (*b*), (*d*) Side views, two unit cells along **b** are drawn, infinite sheets of Mo_6O_{22} clusters are seen. The oxygen octahedra are outlined.

Table 1. *Lattice parameters of the average structure and the components of the modulation wavevector* **q** ($|\mathbf{q}| = 1/\lambda$) *in fractions of* **a***, **b***, **c***

$\mathbf{a}\cdot\mathbf{a}^* = \mathbf{b}\cdot\mathbf{b}^* = \mathbf{c}\cdot\mathbf{c}^* = 1$. Standard deviations in the least significant digit are given in parentheses.

	$K_{0.3}MoO_3$ (192 K)	$K_{0.3}MoO_3$ (100 K)		$Rb_{0.3}MoO_3$ (100 K)	
	Small crystal	Small crystal	Larger crystal	Small crystal	Larger crystal
a (Å)	18.211 (2)	18.164 (2)	18.162 (2)	18.542 (3)	18.536 (2)
b (Å)	7.555 (1)	7.556 (1)	7.554 (1)	7.560 (2)	7.556 (2)
c (Å)	9.834 (1)	9.816 (1)	9.816 (1)	10.037 (1)	10.035 (1)
β (°)	117.51 (1)	117.39 (1)	117.39 (1)	118.51 (1)	118.52 (1)
q_x			0		0
q_y			0.748		0.748
q_z			½		½

Table 2. *Total number of reflections, number of inequivalent reflections, number of inequivalent reflections with* $I > 2.5\sigma(I)$ *and the internal consistency,* R_I

$R_I = \sum_j\{N_j\sum_i[(\langle I\rangle_j - \langle I\rangle_{i,j})^2/\sigma^2_{I,i,j}]\}^{1/2}/\sum_j\{(N_j-1)\sum_i[I^2_{i,j}/\sigma^2_{I,i,j}]\}^{1/2}$ with $\sum_j$ = summation over all independent reflections and $\sum_i$ = summation over all (N_j) symmetrically equivalent reflections for unique reflection j.

	Measured	Unique	With $I > 2.5\sigma(I)$	R_I
K bronze, 192 K				
All reflections	13164	6582	5702	0.090
K bronze, 100 K				
Main reflections	13116	6560	5769	0.085
First-order satellites				
Even k	4898	2379	1473	0.068
Odd k	1790	1790	743	
All reflections	19804	10729	7985	
Rb bronze, 100 K				
Main reflections	7986	4033	3159	0.048
First-order satellites				
Even k	7647	3825	1074	0.19
Odd k	5030	2514	225	0.45
All reflections	20663	10372	4458	

3. Structure determination of the blue bronzes

The modulated structure (with wavevector **q** of length $q = 1/|\lambda|$) is described by specifying the structural parameters (positions $\mathbf{x}_0$, occupation P_0 and temperature factors β_{ij}) in the average unit cell and by specifying for each atom μ the modulation function $\mathbf{u}^\mu$. The modulation is a periodic function of the coordinate in the fourth dimension, $\bar{x}_4$, with $\bar{x}_4 = \mathbf{q}\cdot\mathbf{r}_0$, $\mathbf{r}_0 = \mathbf{n} + \mathbf{x}_0$ being the average position in the **n**th cell. The symmetry in this four-dimensional space is

described by superspace groups (de Wolff, Janssen & Janner, 1981; Janner, Janssen & de Wolff, 1983). A four-dimensional superspace group is given by the group of operators $(\mathfrak{R}, \varepsilon|\boldsymbol{\tau})$ where $\mathfrak{R}$ represents a point-group operation on the three-dimensional part and ε transforms the one-dimensional internal space, with $\boldsymbol{\tau} = (\tau_x, \tau_y, \tau_z, \tau_4)$ the four-dimensional translational part of the operator. We give the superspace symmetry and determine, besides the usual structural parameters such as atomic coordinates x_0, y_0, z_0 and temperature factors, the displacive modulation amplitudes u_i^μ.

The symmetry of the blue bronze is established as follows. From space group $C2/m$ for the average structure, the form $(1,\beta,\frac{1}{2})$, $\beta = 0.748$ for the modulation wavevector leads to the four-dimensional Bravais class $C_1^{C2/m}\Upsilon$. To analyse the systematic extinctions, it is necessary to transform the subcell in such a way that only the irrational components of the modulation wavevector remain. The required transformation, from now on to be adopted, is: $A = a$, $B = b$, $C = 2c$ giving $\mathbf{q} = 0.748\mathbf{b}^*$. The indices of the reflections, $hklm$, are then transformed accordingly to: $H = h$, $K = k$, $L = 2l + m$, $M = m$. The systematic extinctions are : $H + K + M =$ odd for all reflections, which gives the centrosymmetric superspace group $C_1^{C2/m}\Upsilon$. We adopt the common choice in the literature for $\mathbf{q}$, $\mathbf{q} = 0.748\mathbf{b}^*$. However, the description of the modulated structure with $\mathbf{q}' = (1 - q_y)\mathbf{b}^* = 0.252\mathbf{b}^*$ lying in the first Brillouin zone is also possible (by the transformation $H' = H$, $K' = K + M$, $L' = L$, $M' = -M$ and with extinctions $H' + K' =$ odd).

In Fig. 3 we have drawn the symmetry operations in the unit cell. We see that two different types of twofold axes (2_1) and (2_s) are present. The reason that we have put the twofold rotation axis (2_s) (this is a twofold rotation in ordinary three-dimensional space, accompanied by a translation of $\frac{1}{2}$ in the fourth dimension) at the origin, is that we want to describe the structure in the same setting as used by Graham & Wadsley (1966). This means that the $Mo_{10}O_{30}$ cluster is at the origin and thus the K(1) atom is at $Z = \frac{1}{4}$ (formerly $z = \frac{1}{2}$). In the average structure these fragments both lie on twofold axes, but as we see in Fig. 3 these axes become different in nature in the modulated structure. From the structure refinement it becomes clear that the $Mo_{10}O_{30}$ cluster lies on a (2_s) axis and the K(1) atom on a (2_1) axis and therefore we use the alternative setting of the superspace group with (2_s) at the origin: $C_s^{C2/m}\Upsilon$. [When $C_1^{C2/m}\Upsilon$ is preferred all coordinates must be transformed with $Z' = Z - \frac{1}{4}$ and K(1) at the origin.] We give the symmetry operators and corresponding equivalent positions in the centrosymmetric superspace group $C_s^{C2/m}\Upsilon$:

$$(E, 1|n_x n_y n_z n_4), (E, 1|\tfrac{1}{2}\tfrac{1}{2}0\tfrac{1}{2})+, (E, 1|00\tfrac{1}{2}\tfrac{1}{2})+, (E, 1|\tfrac{1}{2}\tfrac{1}{2}\tfrac{1}{2}0)+ (2_y, 1|000\tfrac{1}{2}), (m_y, \bar{1}|000\tfrac{1}{2}), (i, \bar{1}|0000), \quad (1)$$

$$(0,0,0,0); (\tfrac{1}{2},\tfrac{1}{2},0,\tfrac{1}{2})+; (0,0,\tfrac{1}{2},\tfrac{1}{2})+; (\tfrac{1}{2},\tfrac{1}{2},\tfrac{1}{2},0)+ (x,y,z,x_4), (\bar{x},y,\bar{z},x_4+\tfrac{1}{2}), (x,\bar{y},z,-x_4+\tfrac{1}{2}), (\bar{x},\bar{y},\bar{z},-x_4). \quad (2)$$

We consider one modulation type: a displacive one for all atoms. An occupational modulation is excluded because the compound was found to be strictly stoichiometric (refinements with an occupational modulation for the K atoms show that this is true). To analyse the modulated structure we use the following notation for the modulation wave for the μth atom:

$$u_i^\mu(\bar{x}_4^\mu) = u_i^{\mu,c}\cos(2\pi\bar{x}_4^\mu) + u_i^{\mu,s}\sin(2\pi\bar{x}_4^\mu), \quad i = x,y,z, \quad (3)$$

with u_i^μ the first-harmonic Fourier amplitude components of the displacive modulation wave of atom μ, as we have observed only first-order satellite reflections. For a displacive modulation the positions of the atoms are given by

$$\mathbf{r}^\mu(\bar{x}_4^\mu) = \mathbf{r}_0^\mu + \mathbf{u}^\mu(\bar{x}_4^\mu) = \mathbf{n} + \mathbf{x}_0^\mu + \mathbf{u}^\mu(\bar{x}_4^\mu), \quad (4)$$

where $\mathbf{n}$ (n_x,n_y,n_z) is a basic structure-lattice translation, $\mathbf{x}_0^\mu$ is the average position within the basic unit cell.

In superspace symmetry not only the classical parameters are restricted [for example K(1) on $\frac{1}{2},0,\frac{1}{4}$] but modulation parameters are restricted as well. A list of the allowed modulation functions is given in Table 3.

We did the refinement for the average structure and for the modulation with the least-squares program *REMOS*85 (Yamamoto, 1985), which calculates the structure factors in the higher-dimensional analysis, refining besides the 'classical' parameters

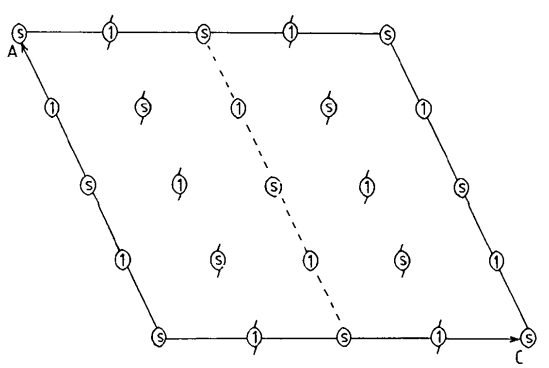

Fig. 3. One supercell (with doubled c axis) is drawn and positions of all 2 and 2_1 axes in superspace group $C_s^{C2/m}\Upsilon$ $(0,\beta,\frac{1}{2})$ are given. The basic unit cell is given by the broken line. Translations along the fourth dimension are indicated by 1 ($\tau_4 = 0$) or s ($\tau_4 = \frac{1}{2}$).

Table 3. *Symmetry restrictions on the components of the modulation function*

Indicated is whether a particular component is even, odd, zero or not restricted.

Atom	Component	Symmetry
K(1)	u_x, u_z	Zero
	u_y	Even
O(1)	u_x, u_y, u_z	Odd
K(2), Mo(1), O(2), O(3)	u_x, u_z	Odd
O(4), O(5), O(6), O(7)	u_y	Even
Mo(2), Mo(3), O(8) O(9), O(10), O(11)	u_x, u_y, u_z	None

the modulation parameters as well. Refinement of the variables, with one extra parameter describing the secondary extinction, was performed by minimizing R_{F^2}. The definition of the R factors is

$$R_F = \sum w||F_{obs}| - |F_{calc}||/\sum w|F_{obs}| \quad (5)$$

and

$$R_{F^2} = [\sum w(|F_{obs}| - |F_{calc}|)^2/\sum w|F_{obs}|^2]^{1/2}. \quad (6)$$

The atomic scattering factors and the anomalous-dispersion factors were taken from *International Tables for X-ray Crystallography* (1974, Vol. IV).

The calculation was started with the results of Graham & Wadsley (1966) for the average structure and with the model of Sato *et al.* (1985) for the Mo displacements. For all reflections unit weights were taken. The final refinement results are listed in Table 4 (R factors) and Table 5 (positional and modulation parameters). The list of temperature factors has been deposited.*

4. Structure of the red bronzes

To compare the blue and red bronzes we did a structure recalculation of the red bronzes from the published observed structure factors (Stephenson & Wadsley, 1965; Mumme & Watts, 1970) by a full-matrix least-squares refinement with the *XTAL* system (Hall & Stewart, 1987), refining the population of the alkali atom as well. These calculations give final R_F factors for both '$K_{0.26}MoO_3$' and '$Cs_{0.25}MoO_3$' of 0.11. The resulting atomic positions are listed in Table 6. The structures of the red bronzes are given in Fig. 2, which shows the two different building blocks of Mo_6O_{22} clusters in the two red bronzes. The structure of '$K_{0.26}MoO_3$' is isotypic with $Cs_{0.33}MoO_3$ (Tsai, Potenza & Greenblatt, 1987). From the structure recalculations

* Lists of structure factors, anisotropic thermal parameters and figures showing the coordination of the Mo and K atoms have been deposited with the British Library Document Supply Centre as Supplementary Publication No. SUP 55454 (183 pp.). Copies may be obtained through The Technical Editor, International Union of Crystallography, 5 Abbey Square, Chester CH1 2HU, England.

Table 4. *The R_F and R_{F^2} values of the refinement for the final results*

Also given are the number of parameters (n_p) and the number of reflections (n_r) used.

	R_F	R_{F^2}	n_p	n_r
K blue bronze, 192 K				
Overall	0.030	0.051	114	5702
K blue bronze, 100 K				
$m = 0$	0.031	0.044	114	5769
$m = 1$	0.049	0.056	64	2216
Overall	0.032	0.044	178	7985
Rb blue bronze, 100 K				
$m = 0$	0.026	0.031	114	3159
$m = 1$	0.108	0.146	64	1299
Overall	0.032	0.034	178	4458

of the red bronzes it follows that, just as in the blue bronzes, the alkali sites in the red bronzes '$K_{0.26}MoO_3$' and '$Cs_{0.25}MoO_3$', are fully occupied and therefore the correct formula for these compounds must be $A_{0.33}MoO_3$.

5. Discussion

Throughout this discussion we refer for coordinates and directions to the Graham & Wadsley (1966) cell choice with a doubled c axis.

Interatomic distances in the average structure at 100, 192 *and* 298 K

When we compare the atomic positions in the average structure at 100 and 192 K (see Table 5) with the room-temperature structure (Ghedira *et al.*, 1985), we can conclude that all values for the room-temperature structure are only slightly different at low temperature. Drastic changes in bond distances are not observed. No strong metal–metal bonds are found at either room temperature or low temperatures (shortest Mo–Mo separation is 3.18 Å, $d_{bond} \simeq$ 2.85 Å).

As was already observed by Ghedira *et al.* (1985), the thermal linear expansion along **b** is almost zero, it is intermediate along [10$\bar{1}$] (parallel to the slabs) and large along [101] (perpendicular to the slabs). This contraction results in smaller distances between the slabs on cooling.

The distances between the Mo and K atoms and their nearest-neighbour O atoms and the Mo–Mo distances are given in Table 7. It is seen that the Mo–O distances vary over a wide range (1.687–2.344 Å). While the Mo(1) octahedron resembles a (2 + 2 + 2) coordination (two short, two intermediate and two long), the Mo(2) and Mo(3) octahedra have a (1 + 4 + 1) coordination. The average Mo–O distances for Mo(1), Mo(2) and Mo(3) at 100 K are 1.984, 1.962 (2×) and 1.962 (2×) Å, respectively, which gives 1.966 Å as the overall average. At 192 K these Mo–O distances are 1.983, 1.963 and 1.963 Å,

Table 5. *Final values for the atomic positions of the average structure and for the amplitudes of the modulation functions*

Upper line for K bronze and lower for Rb bronze.

		192 K	100 K				192 K	100 K		
		x_i^μ	$x_{0,i}^\mu$	$u_i^{\mu,c}$	$u_i^{\mu,s}$		x_i^μ	$x_{0,i}^\mu$	$u_i^{\mu,c}$	$u_i^{\mu,s}$
K(1), Rb(1)						O(4)				
	x	$\frac{1}{2}$	$\frac{1}{2}$	0	0	x	0.0806 (2)	0.0804 (1)	0	−0.0002 (4)
			$\frac{1}{2}$	0	0			0.0789 (2)	0	−0.0014 (7)
	y	0	0	−0.0043 (4)	0	y	$\frac{1}{2}$	$\frac{1}{2}$	−0.0017 (9)	0
			0	−0.0043 (3)	0			$\frac{1}{2}$	−0.002 (2)	0
	z	$\frac{1}{4}$	$\frac{1}{4}$	0	0	z	−0.0053 (2)	−0.0056 (1)	0	−0.0011 (4)
			$\frac{1}{4}$	0	0			−0.0037 (2)	0	−0.0018 (8)
K(2), Rb(2)						O(5)				
	x	0.31174 (7)	0.31163 (4)	0	−0.0004 (1)	x	0.0893 (2)	0.0891 (1)	0	−0.0014 (4)
			0.31563 (3)	0	−0.0001 (1)			0.0884 (2)	0	−0.0023 (7)
	y	$\frac{1}{2}$	$\frac{1}{2}$	−0.0020 (3)	0	y	0	0	−0.0028 (9)	0
			$\frac{1}{2}$	−0.0027 (2)	0			0	−0.000 (2)	0
	z	0.14058 (6)	0.14074 (4)	0	−0.0001 (1)	z	−0.0033 (2)	−0.0034 (1)	0	−0.0017 (4)
			0.14226 (3)	0	0.0001 (1)			−0.0039 (2)	0	−0.0019 (8)
Mo(1)						O(6)				
	x	0.22619 (2)	0.22647 (1)	0	0.00103 (4)	x	−0.1556 (2)	−0.1555 (1)	0	0.0012 (4)
			0.22432 (2)	0	0.00122 (6)			−0.1561 (2)	0	0.0011 (6)
	y	0	0	−0.0027 (1)	0	y	0	0	−0.0004 (9)	0
			0	−0.0033 (2)	0			0	−0.002 (1)	0
	z	0.08708 (2)	0.08728 (1)	0	0.00119 (4)	z	−0.1560 (2)	−0.1561 (1)	0	−0.0007 (4)
			0.08740 (2)	0	0.00145 (7)			−0.1550 (2)	0	−0.0001 (6)
Mo(2)						O(7)				
	x	0.07989 (1)	0.08019 (1)	−0.00016 (4)	0.00163 (3)	x	−0.1408 (2)	−0.1406 (2)	0	0.0015 (4)
			0.07819 (1)	0.00002 (9)	0.00205 (4)			−0.1422 (2)	0	0.0030 (7)
	y	0.25503 (3)	0.25493 (2)	0.00069 (6)	−0.00124 (8)	y	$\frac{1}{2}$	$\frac{1}{2}$	−0.0022 (9)	0
			0.25567 (3)	0.0010 (1)	−0.0019 (1)			$\frac{1}{2}$	−0.003 (2)	0
	z	−0.02123 (1)	−0.02115 (1)	−0.00026 (4)	0.00074 (3)	z	−0.1651 (2)	−0.1652 (1)	0	−0.0005 (4)
			−0.02054 (1)	−0.00053 (8)	0.00072 (4)			−0.1641 (2)	0	−0.0002 (7)
Mo(3)						O(8)				
	x	−0.13835 (1)	−0.13818 (1)	0.00019 (4)	0.00237 (3)	x	0.1022 (2)	0.1027 (1)	−0.0002 (4)	0.0016 (3)
			−0.13937 (1)	0.00057 (9)	0.00300 (3)			0.0989 (1)	−0.0003 (7)	0.0022 (3)
	y	0.24987 (3)	0.24982 (2)	0.00027 (7)	0.00031 (9)	y	0.2544 (4)	0.2540 (2)	−0.0020 (6)	−0.0007 (8)
			0.24995 (3)	0.0004 (1)	0.0002 (1)			0.2604 (3)	−0.0007 (9)	−0.001 (1)
	z	−0.17319 (1)	−0.17319 (1)	−0.00017 (4)	0.00151 (3)	z	−0.0957 (1)	−0.0956 (1)	−0.0003 (4)	0.0009 (3)
			−0.17181 (1)	−0.00041 (9)	0.00216 (4)			−0.0939 (1)	−0.0006 (7)	0.0017 (4)
O(1)						O(9)				
	x	$\frac{1}{4}$	$\frac{1}{4}$	0	0.0001 (4)	x	0.1858 (1)	0.1861 (1)	−0.0002 (4)	0.0011 (2)
			$\frac{1}{4}$	0	−0.0002 (4)			0.1838 (1)	0.0007 (7)	0.0012 (3)
	y	$\frac{1}{4}$	$\frac{1}{4}$	0	−0.002 (1)	y	0.2436 (3)	0.2437 (2)	−0.0007 (6)	−0.0011 (7)
			$\frac{1}{4}$	0	−0.003 (2)			0.2427 (3)	0.0011 (9)	−0.002 (1)
	z	$\frac{1}{4}$	$\frac{1}{4}$	0	0.0012 (4)	z	0.0805 (1)	0.0809 (1)	−0.0001 (3)	0.0005 (2)
			$\frac{1}{4}$	0	0.0019 (5)			0.0807 (1)	0.0008 (7)	0.0005 (4)
O(2)						O(10)				
	x	0.2507 (2)	0.2509 (2)	0	−0.0008 (5)	x	−0.0877 (2)	−0.0874 (1)	0.0001 (3)	0.0003 (3)
			0.2492 (2)	0	−0.0006 (6)			−0.0889 (1)	−0.0001 (5)	0.0005 (4)
	y	0	0	−0.0033 (9)	0	y	0.2192 (3)	0.2194 (2)	−0.0021 (7)	0.0014 (6)
			0	−0.003 (1)	0			0.2198 (3)	−0.003 (1)	0.001 (1)
	z	0.0130 (2)	0.0130 (1)	0	0.0001 (4)	z	−0.2259 (1)	−0.2261 (1)	−0.0001 (3)	−0.0003 (3)
			0.0156 (2)	0	0.0006 (6)			−0.2223 (1)	0.0002 (5)	−0.0004 (4)
O(3)						O(11)				
	x	0.3191 (2)	0.3196 (1)	0	0.0018 (4)	x	−0.0375 (1)	−0.0374 (1)	−0.0001 (4)	0.0009 (2)
			0.3164 (2)	0	0.0021 (6)			−0.0378 (1)	0.0006 (8)	0.0008 (4)
	y	0	0	−0.0034 (9)	0	y	0.2462 (3)	0.2460 (2)	−0.0018 (6)	0.0012 (7)
			0	−0.005 (1)	0			0.2457 (3)	−0.0047 (9)	0.001 (1)
	z	0.1678 (2)	0.1681 (1)	0	0.0001 (4)	z	−0.0732 (1)	−0.0733 (1)	0.0000 (3)	−0.0004 (2)
			0.1684 (2)	*0*	*0.001 (7)*			*−0.0721 (1)*	*−0.0011 (7)*	*−0.0001 (4)*

with 1.967 Å as the overall average. All these distances are larger than at room temperature ($d_{overall}$ = 1.965 Å); between 298 K and T_c the average Mo–O distances in the Mo(2) and Mo(3) octahedra lengthen, while they remain the same below T_c. The changes (Δ) in the distance between Mo and the nearest O atoms are responsible for this expansion: Mo(1)–O(2) with Δ = +0.02 Å, Mo(2)–O(8) with Δ = +0.01 Å, Mo(3)–O(10) with Δ = +0.01 Å, which are balanced in the Mo(1) octahedron only by Mo(1)–O(6) with Δ = −0.02 Å.

All K–O distances become significantly shorter on cooling, mainly between 298 K and T_c, because of a decrease of the distance between the slabs. The overall average K–O distance in a tenfold coordination decreases from 3.030 Å at 298 K to 3.018 Å at 192 K and 3.012 Å at 100 K. All these distances refer to the K compound. The same behaviour, except for the

Table 6. *Fractional atomic coordinates of* '$K_{0.26}MoO_3$' *and* '$Cs_{0.25}MoO_3$'

'$K_{0.26}MoO_3$': $a = 14.278$, $b = 7.723$, $c = 6.386$ Å, $\beta = 92.57°$, space group $C2/m$. '$Cs_{0.25}MoO_3$': $a = 6.425$, $b = 7.543$, $c = 8.169$ Å, $\beta = 96.5°$, space group $P2_1/m$. Refinement of the alkali content confirmed the formula $A_{0.33}MoO_3$ for both compounds.

	K red bronze			Cs red bronze		
μ	x	y	z	x	y	z
K, Cs	0.3158 (7)	0	0.164 (2)	0.1789 (9)	$\frac{3}{4}$	0.6114 (7)
Mo(1)	0.1230 (2)	0	0.6404 (5)	0.3483 (9)	$\frac{1}{4}$	0.7752 (8)
Mo(2)	0.0599 (2)	0.2615 (4)	0.2691 (3)	0.2715 (5)	0.0046 (7)	0.1061 (5)
O(1)	0	0.270 (5)	0	0	0	0
O(2)	0.223 (2)	0	0.514 (5)	0.293 (9)	$\frac{1}{4}$	0.040 (7)
O(3)	0.148 (2)	0	0.902 (5)	0.309 (9)	$\frac{3}{4}$	0.088 (7)
O(4)	0.544 (2)	0	0.293 (5)	0.466 (9)	$\frac{1}{4}$	0.599 (7)
O(5)	0.043 (2)	0	0.308 (5)	0.101 (9)	$\frac{1}{4}$	0.725 (7)
O(6)	0.172 (1)	0.257 (4)	0.201 (3)	0.396 (6)	0.006 (6)	0.859 (5)
O(7)	0.084 (1)	0.241 (4)	0.588 (3)	0.225 (6)	0.042 (7)	0.306 (5)

longer interatomic distances, occurs with the Rb blue bronze.

The behaviour of an $Mo_{10}O_{30}$ cluster on cooling can best be studied by considering the Mo–Mo distances. As can be seen from Table 7 the average Mo–Mo distance within a cluster shortens on cooling; this comes from the shared-edge distances, while the shared-corner distances remain constant. On the other hand, the Mo–Mo distances between clusters lengthen on cooling. We remark that the shared-corner distances inside a cluster are longer than between clusters. So, as the Mo–O distances become modulated and their overall average distances become longer, the $Mo_{10}O_{30}$ cluster as a whole shrinks on cooling.

The structural dimensionality of the blue bronze at 100 and 192 K is that of a one-dimensional K sublattice, a two-dimensional Mo sublattice and a three-dimensional oxygen sublattice. An infinite number of chains of corner-sharing MoO_6 octahedra run along the b axis and along the [101] direction. The different number of chains of MoO_6 octahedra per unit cell along **b** and [101] and the difference in overlap in the two directions can explain qualitatively the anisotropy in the electrical conductivity. However, the quasi-one-dimensional metallic properties cannot be understood from the average structure.

Charge distribution in the average structure on the Mo *sites*

The charge distributrion (Mo^{5+}/Mo^{6+}) on the Mo sites is calculated by analysing the Mo–O distances. The bond strength of each individual Mo–O bond has been calculated by the use of the Zachariasen (1978) formula

$$D_i = D(1)[1 - B \ln s_i] \quad (7)$$

where D_i is the interatomic distance, $B = 0.166$ is a constant, s_i is the individual bond strength and $D(1)$ is the atomic distance for unit strength. The sum of the bond strengths $\sum s_i$ is equal to the valence (or charge) of the central cation. The structure refinement shows full occupancy of the alkali sites. With the assumption of bond numbers 2 for O and 1 for K this determines the average positive charge on Mo to be $+5.700$ ($K^+_{0.3}Mo^{5.7+}O^{2-}_3$). Generally, the interatomic distances change with temperature as a result of thermal expansion and distortions. Therefore, the parameter $D(1)$ will also depend on the temperature. We have chosen at each temperature a value of $D(1)$ such that the average valence of Mo is $+5.700$. With these values of $D(1)$ the valences (charges) of Mo(1), Mo(2) and Mo(3) can be calculated. We give the distribution of the Mo $5d$ electrons over the Mo sites at 100, 192 and 298 K in Table 8. The values deduced in this way for $D(1)$ are reasonable. The value proposed by Zachariasen for Mo–O bonds is 1.89 Å. At 298 K we calculate different values for the K, Rb and Tl blue bronze, while in the semiconducting state they become nearly equal. The differences at 298 K are ascribed to polarization effects.

The calculated charge distributions show that most of the Mo $4d$ electrons are located on the Mo(2) and Mo(3) sites. Only a small fraction of the $4d$ electrons are located at Mo(1) sites (10% in $K_{0.3}MoO_3$ at 298 K); these sites are isolated and the $4d$ electrons at Mo(1) presumably do not contribute to the electrical conductivity. With the lowering of the temperature we observe in the average structure of the K bronze a transfer of some $4d$ electrons from the Mo(2) and Mo(3) sites to the Mo(1) site [the distribution of Mo^{5+} in $K_{0.3}MoO_3$ at 192 and 100 K in the average structure over the Mo(1), Mo(2) and Mo(3) sites is 12, 45, 43% and 13, 44, 43%, respectively]. However, this cannot explain the metal-to-semiconductor transition because in the Rb blue bronze approximately the same charge distribution is calculated at room temperature (15, 43, 42%) and in Tl blue bronze an even higher charge distribution on the Mo(1) is found (17, 40, 43%) (Ganne, Boumaza, Dion & Dumas, 1985) at room temperature, although both compounds have one-dimensional metallic properties. Moreover, in the semiconducting state of the Rb bronze, just the opposite charge transfer [from Mo(1) to Mo(2) and Mo(3)] is observed.

The modulated structure and its charge distribution

The modulation amplitudes of the K and Rb compound differ only slightly (see Table 5). However, the standard deviations for the K compound are lower than for the Rb compound, where the measurements were more affected by absorption. We will therefore discuss here primarily the K blue

Table 7. *Interatomic distances and bond strengths, s, in the blue bronzes at different temperatures*

Distances at 298 K taken from Ghedira *et al.* (1985). Upper line for K bronze and lower line for Rb bronze.

	100 K		192 K		298 K	
	Distance	*s*	Distance	*s*	Distance	*s*
Octahedron Mo(1)						
O(2)	1.709 (4)	1.798	1.709 (5)	1.800	1.690 (3)	1.882
	1.710 (5)	1.795			1.714 (7)	1.765
O(3)	1.705 (2)	1.821	1.703 (3)	1.834	1.698 (3)	1.835
	1.703 (3)	1.836			1.700 (7)	1.846
O(5)	2.304 (1)	0.271	2.298 (3)	0.276	2.310 (3)	0.260
	2.302 (3)	0.273			2.313 (6)	0.262
O(6)	2.256 (3)	0.315	2.257 (4)	0.315	2.276 (3)	0.290
	2.254 (5)	0.318			2.262 (6)	0.309
O(9) × 2	1.964 (2)	0.799	1.964 (2)	0.800	1.962 (2)	0.790
	1.963 (2)	0.803			1.964 (4)	0.797
Average distance, Σs	1.984	5.802	1.983	5.824	1.983	5.848
	1.983	5.829			1.986	5.775
Octahedron Mo(2)						
O(8)	1.689 (2)	1.916	1.692 (4)	1.800	1.677 (2)	1.962
	1.690 (4)	1.913			1.686 (5)	1.930
O(11)	1.898 (2)	0.985	1.898 (2)	0.986	1.896 (2)	0.976
	1.891 (2)	1.010			1.892 (4)	1.002
O(11)	2.318 (2)	0.259	2.318 (2)	0.259	2.319 (2)	0.253
	2.314 (2)	0.263			2.318 (4)	0.258
O(4)	1.876 (1)	1.057	1.876 (1)	1.058	1.873 (2)	1.050
	1.877 (1)	1.056			1.874 (2)	1.061
O(5)	1.951 (1)	0.832	1.952 (1)	0.831	1.952 (1)	0.816
	1.955 (1)	0.824			1.954 (4)	0.822
O(9)	2.043 (1)	0.621	2.041 (1)	0.626	2.045 (2)	0.606
	2.043 (2)	0.623			2.049 (4)	0.608
Average distance, Σs	1.962	5.670	1.963	5.660	1.960	5.663
	1.963	5.688			1.962	5.681
Octahedron Mo(3)						
O(10)	1.693 (2)	1.892	1.692 (4)	1.900	1.682 (2)	1.931
	1.691 (3)	1.907			1.683 (5)	1.948
O(9)	2.345 (2)	0.238	2.351 (2)	0.233	2.348 (2)	0.231
	2.338 (2)	0.244			2.347 (7)	0.235
O(1)	1.892 (1)	1.004	1.892 (1)	1.005	1.890 (1)	0.994
	1.897 (1)	0.991			1.894 (1)	0.995
O(7)	1.899 (1)	0.982	1.899 (1)	0.983	1.897 (1)	0.972
	1.900 (1)	0.981			1.898 (1)	0.983
O(6)	1.968 (1)	0.789	1.969 (1)	0.787	1.964 (1)	0.785
	1.970 (1)	0.785			1.989 (2)	0.736
O(11)	1.974 (1)	0.774	1.976 (1)	0.770	1.979 (2)	0.749
	1.989 (2)	0.739			1.969 (4)	0.784
Average distance, Σs	1.962	5.678	1.963	5.678	1.960	5.662
	1.964	5.647			1.963	5.682

	100 K	192 K	298 K
Polyhedron K(1)			
O(8) × 4	3.305 (2)	3.301 (2)	3.304 (2)
	3.313 (3)		3.325 (5)
O(10) × 4	2.814 (2)	2.824 (3)	2.839 (2)
	2.896 (3)		2.923 (5)
O(3) × 2	2.911 (2)	2.923 (3)	2.941 (3)
	2.992 (3)		3.009 (7)
Average	3.030	3.035	3.045
	3.082		3.101
Inside $Mo_{10}O_{30}$ units			
Edge-shared			
Mo(1)—Mo(2)	3.178 (1)	3.179 (1)	3.181 (1)
	3.189 (1)		3.190 (1)
Mo(1)—Mo(3)	3.387 (1)	3.390 (1)	3.395 (1)
	3.387 (1)		3.394 (1)
Mo(2)—Mo(2)	3.377 (1)	3.378 (1)	3.377 (1)
	3.372 (1)		3.371 (1)
Mo(2)—Mo(3)	3.460 (1)	3.463 (1)	3.471 (1)
	3.467 (1)		3.477 (1)

	100 K	192 K	298 K
Polyhedron K(2)			
O(8) × 2	2.857 (2)	2.864 (4)	2.885 (2)
	2.966 (4)		2.983 (5)
O(9) × 2	2.804 (2)	2.812 (2)	2.822 (2)
	2.899 (2)		2.903 (4)
O(10) × 2	2.921 (2)	2.922 (2)	2.932 (3)
	2.948 (2)		2.964 (5)
O(2)	2.692 (3)	2.693 (3)	2.703 (3)
	2.802 (4)		2.811 (7)
O(7)	3.355 (4)	3.362 (5)	3.379 (3)
	3.447 (4)		3.476 (7)
O(1) × 2	3.411 (1)	3.420 (1)	3.436 (1)
	3.499 (1)		3.529 (1)
Average	3.003	3.009	3.023
	3.087		3.105
Between $Mo_{10}O_{30}$ units			
Corner-shared			
Mo(2)—Mo(2)	3.704 (1)	3.702 (1)	3.689 (1)
	3.694 (1)		3.689 (1)
Mo(3)—Mo(3)	3.781 (1)	3.784 (1)	3.774 (1)
	3.781 (1)		3.777 (1)
Mo(3)—Mo(3)	3.785 (1)	3.780 (1)	3.780 (1)
	3.794 (1)		3.788 (1)
Average	3.757	3.755	3.750
	3.756		3.751

Table 7 (*cont.*)

	100 K	192 K	298 K
Average	3.351	3.353	3.356
	3.354		3.358

	100 K	192 K	298 K
Inside $Mo_{10}O_{30}$ units			
Corner-shared			
Mo(2)—Mo(2)	3.853 (1)	3.854 (1)	3.854 (1)
	3.866 (1)		3.866 (1)
Mo(3)—Mo(3)	3.775 (1)	3.776 (1)	3.776 (1)
	3.779 (1)		3.778 (1)
Mo(2)—Mo(3)	3.708 (1)	3.709 (1)	3.708 (1)
	3.715 (1)		3.713 (1)
Average	3.779	3.780	3.779
	3.787		3.786

Table 8. *D*(1) *values and charge* (n_d) *distributions on the* Mo *sites at* 100, 192 *and* 298 K *for the blue bronzes*

The last column gives the corresponding values for $Cs_{0.33}MoO_3$ red bronze.

	100 K		192 K	298 K			298 K
	K	Rb	K	K	Rb	Tl	Cs
D(1)	1.893	1.894	1.894	1.888	1.893	1.902	1.897
n_d [Mo(1)]	0.198	0.171	0.176	0.152	0.225	0.255	0.127
n_d [Mo(2)]	0.330	0.312	0.340	0.337	0.319	0.296	0.436
n_d [Mo(3)]	0.322	0.353	0.322	0.338	0.318	0.326	

bronze and point out afterwards some differences with the Rb bronze.

The largest modulation amplitudes are on Mo(2) and Mo(3), forming the infinite chain along *b*, and these are in phase with each other with amplitudes of about 0.03 and 0.05 Å, in directions approximately parallel to [221] and [201], respectively. The modulation amplitudes of these atoms along **b** are small. Modulation displacements of atoms in neighbouring layers are in antiphase. The Mo(1) displacement is along [121] and its *ac* component is in phase with the Mo(2), Mo(3) distortion. The Mo(1) atom is located on the outside of the cluster and has a considerable component along **b**, with a phase difference of 90°. Generating all symmetrically equivalent atoms in the unit cell shows that all Mo atoms in a slab at the same height in the chain distort within the *ac* plane in nearly the same direction; atoms in neighbouring slabs displace in the opposite direction (Fig. 4). The model for the Mo-atom displacements proposed by Sato *et al.* (1985) agrees with this overall picture.

The alkali atoms K(1) and K(2) displace along **b** only, with amplitudes 0.03 and 0.02 Å, respectively. Together with these K modulations, the Mo(1) displacement and those of the neighbouring O atoms on the outside of a cluster occur in phase, along **b**. This can conveniently be seen from Table 5 in which the coordinates of all independent atoms are taken at the same side of a cluster in the unit cell. When all atoms on one side of a cluster displace downwards, they move upwards at the other side. After about two clusters along **b** just the opposite occurs (Fig. 5). This correlation between the K, O and Mo(1) atoms results in a rotation of clusters along [101], being a longitudinal (parallel to **b**) distortion that is 90° out of phase with the transversal displacements of the

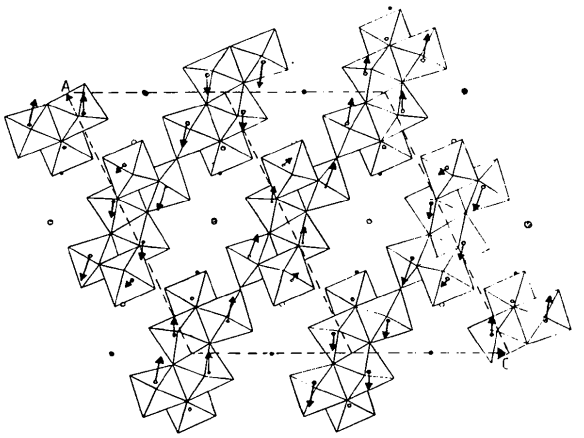

Fig. 4. Amplitudes and directions of Mo modulations in $K_{0.30}MoO_3$ at 100 K perpendicular to **b**. The lengths of the arrows are enlarged 50 times.

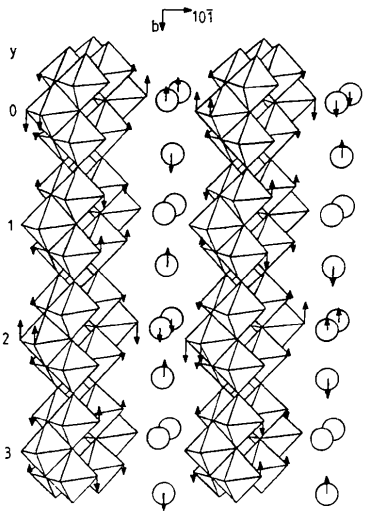

Fig. 5. Amplitudes and directions of K-atom and closest coordinated O-atoms modulations in a view along [101]. The lengths of the arrows are enlarged 50 times.

Mo atoms. Appreciable O-atom displacements are also present in the *xz* plane (for example $|\mathbf{u}^{O(5)}| = 0.04$ Å along [101]), but this cannot simply be interpreted in terms of a translation or rotation of clusters. Pure translations and rotations of individual octahedra are not observed, probably because the octahedra share both corners and faces with each other.

An overview of the modulation displacements can be obtained by plotting the interatomic distances as a function of the modulation-phase parameter $\varphi = \bar{\mathbf{x}}_4^\mu - \mathbf{q}\cdot\mathbf{x}_0^\mu$ (mod 1). These figures, for the distances Mo–Mo, Mo(1)–O, Mo(2)–O, Mo(3)–O, K(1)–O and K(2)–O, were deposited as Figs. 7–12, respectively. Hardly any variation is found between the nearest neighbouring Mo atoms. The Mo–Mo distances along the chain direction ($\simeq 3.80$ Å) are too long to form metal–metal bonds as in, for example, the compound Mo_2S_3 (Schutte & de Boer, 1993). However, in Mo_2S_3 there are three 4*d* electrons present on each Mo in the chain, *versus* only 0.3 4*d* electrons in the blue bronzes. Inside $Mo_{10}O_{30}$ clusters there may be some small metal bonding present *via* the shared-edge coordinations ($\simeq 3.2$–3.5 Å) but this bonding is, just as for the other distances, hardly affected by the modulation.

Larger variations (maximum 0.05 Å) are found in the Mo–O distances for the three independent Mo sites. For the Mo(2), Mo(3) octahedra the strongest modulation is on the four O atoms at intermediate distance, while for the Mo(1) octahedron the strongest modulation is on the two O atoms with the largest distance. These displacements are not very large, certainly not as large as in the modulated structure of the compound calaverite $AuTe_2$ (Schutte & de Boer, 1988). However, in $AuTe_2$ we proposed a valence fluctuation on the metal between +1 and +3, here the fluctuation will be limited between +5.6 and +5.8. For the K–O distances, the largest distortion is found for the K(1)–O(3) distance, varying between 2.88 and 2.95 Å.

Charge distribution in the modulated structure

We can calculate the charge distributions on the Mo sites as a function of the phase φ of the modulation wave along **b** from the calculated Mo–O interatomic distances in the modulated phase. This charge ordering is given in Fig. 6 for the K bronze and corresponds to the lock-in situation with $q_y = 0.75$. In fact, the modulation wavevector is incommensurable and therefore all intermediate charge distributions on the Mo sites along the chain are present. Whereas at room temperature the Mo atoms have constant valencies along the chain [Mo(1): 5.85, Mo(2): 5.66; Mo(3): 5.66], at 100 K the charge distribution on the Mo(2), Mo(3) atoms within a cluster orders, and especially around $\varphi = 0, \frac{1}{2}$ a clear charge separation occurs (5.60–5.74). Also at about $\varphi = \frac{1}{4}, \frac{3}{4}$ a charge transfer is observed; electrons from the Mo(2) and Mo(3) atoms move from one side of the cluster to the other, resulting in Mo valencies ranging from 5.68–5.71 at one side of the cluster to 5.65–5.66 at the other. No appreciable charge transfer is found between neighbouring clusters.

Apart from the ordering of Mo^{5+}, we calculated a possible charge fluctuation on the K atoms by similar charge calculations for the K polyhedra as carried out for the Mo octahedra. Using the values $D(1) = 1.84$ Å, $B = 0.261$ (given by Brown, 1981) this gives valencies of 0.93 and 1.00 on the K(1) and K(2) atoms, respectively, and is nearly independent of the phase of the modulation wave [ranging for K(1) between 0.92 and 0.93; for K(2) between 1.00 and 1.01]. So there seems to be no valence fluctuation on the alkali atoms, in agreement with the observed Knight shift (Segransan, Janossy, Berthier, Marcus & Butaud, 1986).

Comparison between the blue and red bronzes

The interatomic distances in the recalculated structure of the red bronzes (Table 9) differ significantly from those given by Stephenson & Wadsley (1965) and Mumme & Watts (1970), who assumed the alkali site to be only partly filled. We find that in both red bronzes the alkali sites are fully occupied. The interatomic distances are now very close to those in

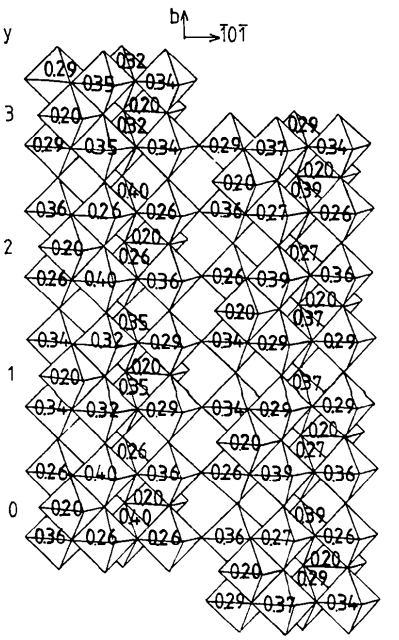

Fig. 6. Schematic diagram (in a view along [10$\bar{1}$]) of the *d*-electron distribution in the K blue bronze at 100 K.

Table 9. *Interatomic distances and bond strengths in the red bronzes*

Distances for $Cs_{0.33}MoO_3$ taken from Tsai *et al.* (1987).

*C*2/*m*, *P*2$_1$/*m*	$K_{0.26}MoO_3$ Distance	$Cs_{0.25}MoO_3$ Distance	$Cs_{0.33}MoO_3$ Distance	*s*
Octahedron Mo(1)				
O(2);O(4)	1.67 (3)	1.70 (1)	1.710 (6)	1.808
O(3);O(5)	1.69 (3)	1.60 (6)	1.697 (3)	1.885
O(5);O(2)	2.37 (3)	2.23 (6)	2.360 (2)	0.229
O(5′);O(3)	2.40 (3)	2.35 (5)	2.365 (3)	0.226
O(7);O(6) × 2	1.96 (3)	1.98 (4)	1.943 (2)	0.863
Average	2.01	1.97	2.00	
Σs				5.873
Octahedron Mo(2)				
O(1);O(1)	1.89 (1)	1.86 (0)	1.880 (1)	1.054
O(4);O(2)	1.86 (1)	1.94 (2)	1.878 (2)	1.061
O(5);O(3)	2.05 (1)	1.94 (1)	2.053 (1)	0.608
O(6);O(7)	1.67 (2)	1.71 (4)	1.682 (2)	1.977
O(7);O(6)	2.06 (2)	2.12 (4)	2.084 (2)	0.551
O(7′);O(6)	2.29 (2)	2.26 (4)	2.262 (2)	0.313
Average	1.97	1.97	1.97	
Σs				5.564
	$K_{0.26}$	$Cs_{0.25}$	$Cs_{0.33}$	
Polyhedron K(1), Cs(1)				
O(2);O(4)	2.64 (3)	3.01 (6)	2.980 (3)	
O(3);O(5)	2.86 (3)	3.11 (5)	3.100 (3)	
O(6);O(7) × 2	2.87 (2)	3.17 (4)	3.181 (2)	
O(6);O(7) × 2	3.01 (2)	3.37 (5)	3.207 (2)	
O(7);O(6) × 2	2.89 (2)	3.02 (4)	3.073 (2)	
Between Mo_6O_{22} units				
Corner-shared				
Mo(2)–Mo(2)	3.685 (5)	3.717 (5)	3.695 (1)	
Mo(2)–Mo(2)	3.769 (3)	3.841 (8)	3.760 (1)	
Inside Mo_6O_{22} units				
Edge-shared				
Mo(1)–Mo(1)	3.212 (3)	3.172 (6)	3.215 (1)	
Mo(1)–Mo(2)	3.372 (4)	3.358 (7)	3.356 (1)	
Mo(2)–Mo(2)	3.475 (3)	3.575 (5)	3.483 (1)	
Mo(1)–Mo(1)	3.872 (4)		3.845 (1)	
Corner-shared				
Mo(2)–Mo(2)	4.039 (5)	3.841 (8)	4.034 (1)	

$Cs_{0.33}MoO_3$, as determined recently by Tsai, Potenza & Greenblatt (1987) (Table 9). One could make the same bond-strength calculation as was made for the blue bronzes but the structural parameters are still not precise enough to obtain reliable bond strengths (standard deviations in the interatomic distances are larger than 0.01 Å). Therefore, we use the values of the recently determined $Cs_{0.33}MoO_3$ red bronze.

The semiconducting behaviour of the red bronzes has been interpreted in terms of thermally activated electron hopping from cluster to cluster. The change from the metallic conductivity in the blue bronzes to the semiconducting behaviour in the red bronzes was explained with a formal Mott transition of delocalized into localized states due to a critical overlap between cation–anion–cation orbitals along the Mo–O–Mo chain parallel to **b** (Travaglini & Wachter, 1983). For appropriately short Mo–O distances ($d < 2$ Å), large overlap leads to bands and metallic conductivity, while longer Mo–O distances mean more localized ortbitals and semiconductor behaviour. In the same way the semiconducting properties in the blue bronzes along [101] were understood. An electron has to hop from one cluster to the next because the Mo–O separation is about 2.3 Å.

The metal–semiconductor transition

The conductivity in the blue bronzes along the chain direction can be explained by a band picture with hybridized Mo and O orbitals (overlap of $Mod_{t_{2g}}$–Op_π) based on the ReO_3 model (Goodenough, 1965). The σ and π bonding bands are filled, while the σ^* and π^* antibonding bands are empty. By charge transfer from the alkali metal the π^* band becomes partly filled. The value of the Fermi wavevector $2k_F = \frac{3}{4}b^*$ corresponds with a distortion in which a three-quarter-filled π^* band splits into a full and an empty band. The three-quarter filling is obtained by a complete charge transfer of electrons from the three alkali metals to the doubly degenerate π^* bands of the $Mo_{10}O_{30}$ cluster in $K_3Mo_{10}O_{30}$.

The metal-to-semiconductor transition with its associated nonlinear conductivity properties in the blue bronzes has not been directly explained in terms of critical overlap between orbitals. Suggested models for the transition were Mo–Mo pair formation or *d*-electron transfer to Mo(1) sites (Ghedira *et al.*, 1985). From the present determination of the modulated structure it becomes clear that Mo–Mo pair formation does not occur. Also the small *d*-electron transfer to Mo(1), which we deduced for the K blue bronze, cannot explain the transition.

We will in the following point out how small distortions in the modulated structure can affect the critical overlap between cation–anion–cation orbitals and together with the charge ordering give rise to the localization of conduction electrons along the chain direction and lead to semiconducting properties. The smallest Mo–O separation along a chain that gives rise to localized orbitals is called the critical overlap distance. For larger distances a localized-electron theory applies. We first analyse the Mo–O distances (in Å) for Mo octahedra along the chain parallel to the *b* axis, for both the red and the blue bronzes.

Red Cs bronze:
–O(4)–Mo(2)–O(5)–Mo(2)–O(4)–
at 298 K: –1.878–2.053–2.053–1.878–

Blue K bronze:
–O(4)–Mo(2)–O(5)–Mo(2)–O(4)–; –O(7)–Mo(3)–O(6)–Mo(3)–O(7)–
at 298 K: –1.873–1.952–1.952–1.873–; –1.897–1.964–1.964–1.897–
at 192 K: –1.876–1.952–1.952–1.876–; –1.899–1.969–1.969–1.899–
at 100 K: (each second line is for the chain in the same cluster, related by the twofold axis)

$\varphi = 0$:
–1.890–1.964–1.939–1.863–; –1.906–1.977–1.959–1.892–
–1.863–1.939–1.964–1.890–; –1.892–1.959–1.977–1.906–
$\varphi = \frac{1}{4}$:
–1.895–1.937–1.937–1.895–; –1.913–1.958–1.958–1.913–
–1.858–1.966–1.966–1.858–; –1.885–1.978–1.978–1.885–
$\varphi = \frac{1}{2}$:
–1.863–1.939–1.964–1.890–; –1.892–1.959–1.977–1.906–
–1.890–1.964–1.939–1.863–; –1.906–1.977–1.959–1.892–
$\varphi = \frac{3}{4}$:
–1.858–1.966–1.966–1.858–; –1.885–1.978–1.978–1.885–
–1.895–1.937–1.937–1.895–; –1.913–1.958–1.958–1.913–

For semiconducting behaviour at least one of the distances along the chain should be larger than the critical overlap distance. By comparing the blue and red bronzes at room temperature, the critical overlap distance must be between 1.95 and 2.05 Å [determined by the Mo(2)–O(5) distance]. Now, comparing the Mo–O distances for the K blue bronze between the metallic room-temperature structure and the semiconducting modulated structure we find that the critical overlap distance must be between 1.952 and 1.966 Å. The variation of the Mo(2)–O(5) distance by the modulation along the chain then leads to a very critical change of Mo–O overlap distances. At some phases of the modulation wave, good overlap is present ($d = 1.937$ Å) but at other phases the overlap is not so good ($d = 1.966$ Å). By variation of the modulation phase, the CDW can slide along the chain. Charge transport *via* the Mo(3) chain is less probable because of larger interatomic distances.

The same considerations can be applied to the Rb (and Tl) blue bronze, where we observe nearly the same Mo–O distances along the chain.

Blue Rb bronze:
–O(4)–Mo(2)–O(5)–Mo(2)–O(4)–; –O(7)–Mo(3)–O(6)–Mo(3)–O(7)–
at 298 K: –1.874–1.954–1.954–1.874–; –1.898–1.989–1.989–1.899–
(compare Tl bronze at 298 K: –1.878–1.960–1.960–1.878–; –1.904–1.973–1.973–1.904–)
at 100 K:
$\varphi = 0$:
–1.89–1.94–1.97–1.85–; –1.91–1.99–1.94–1.89–
–1.85–1.97–1.94–1.89–; –1.89–1.94–1.99–1.91–
$\varphi = \frac{1}{4}$:
–1.90–1.94–1.94–1.90–; –1.91–1.95–1.95–1.91–
–1.85–1.98–1.98–1.85–; –1.88–1.98–1.98–1.88–
$\varphi = \frac{1}{2}$:
–1.85–1.97–1.94–1.89–; –1.89–1.94–1.99–1.91–
–1.89–1.94–1.97–1.85–; –1.91–1.99–1.94–1.89–
$\varphi = \frac{3}{4}$:
–1.85–1.98–1.98–1.85–; –1.88–1.98–1.98–1.88–
–1.90–1.94–1.94–1.90–; –1.91–1.95–1.95–1.91–

The values for the Rb bronze are less accurate because of larger standard deviations of the modulation amplitudes. We see that the Rb bronze has the same critical Mo–O overlap range (1.95–1.97 Å) as the K bronze. Together with the modulated charge distribution this probably explains the similar electrical transport properties in the two compounds.

The question remains why the blue bronzes have this incommensurately modulated structure. In other CDW compounds modulated structures are often observed in which short metal–metal chains (< 3.5 Å) are distorted towards the formation of metal pairs or four-metal-atom clusters, as in the compounds $NbTe_4$ (van Smaalen, Bronsema & Mahy, 1986) and Mo_2S_3 (Schutte & de Boer, 1993). In these compounds the modulation wavevector **q** is incommensurate along the chain; there are atomic displacements along the chain direction and the displacements in neighbouring chains are in antiphase. In the blue bronzes incommensurability along the chain and antiphase ordering between the slabs are also present but no metal–metal bonding is observed.

The blue bronzes differ from the other CDW compounds by the smaller number of excess *d* electrons on the metal atom. However, we do not think that this is essential for nonlinear conductivity. More important is the absence of short metal–metal distances. The Mo–Mo distance between cluster units (≃3.7 Å) is too large for direct overlap. In the other CDW compounds valence fluctuations along the chain are induced by variations in metal–metal bonding. In the blue bronzes this is not possible because of the absence of metal–metal bonding. However, in the blue bronzes valence fluctuations on the Mo atoms are the result of variations of Mo–O distances. This is what we observe in the modulated structure of the blue bronze: a variation of Mo–O distances along the chain between 1.94 and 1.97 Å, associated with valence fluctuations of the Mo atoms. This different origin of the Mo valence fluctuations in the blue bronze (by Mo–O bonding) compared with in the other CDW compounds (by Mo–Mo bonding), together with the changing Mo–O orbital overlap along the chain may be related to the nonlinear transport properties in these compounds. Therefore, we suggest that in other compounds that show nonlinear conductivity (such as $NbSe_3$) the presence of charge fluctuations on the metal atom along the chain direction is the result of variations of metal–*nonmetal* (Nb–Se) *bonding [and not by variations of* metal–metal (Nb–Nb) bonding]. In the red bronzes both the Mo–Mo distances (≃3.7 Å) and the Mo–O distances (≃2.0 Å) along the chain direction are too long to give effective overlap and therefore the red bronzes always show semiconducting behaviour.

6. Concluding remarks

We have determined the modulated structure of the semiconducting phase of the blue K and Rb bronzes

at 100 K. The largest modulation amplitudes ($\simeq$0.04 Å) are on Mo(2) and Mo(3) atoms forming the infinite chain along **b**. Their displacements are in the slabs and perpendicular to **b**. Within one slab, all Mo atoms, which are on the same height in the chain, displace in phase. With a phase shift of 90°, the alkali atoms together with their surrounding oxygens displace ($\sim$0.02 Å) in the chain direction. Displacements in neighbouring layers are in antiphase. The same structural features are observed for both the K and and the Rb bronzes.

Charge-distribution calculations in the modulated structure reveal valence fluctuations on the Mo atoms along the chain direction by varying Mo–O bonding. The Mo^{5+} ordering below T_c on the Mo(2), Mo(3) atoms and the charge transfer within the $Mo_{10}O_{30}$ cluster, together with a varying orbital overlap along the chain direction, point to localization of conduction electrons and are probably the origin of the nonlinear transport properties.

This work is part of the research program of the Netherlands Foundation for Chemical Research (SON) and was made possible by financial support from the Netherlands Organisation for the Advancement of Pure Research (ZWO). This work was supported in part by the EC contract No. SC1-0032-C(CD).

References

BOER, J. L. DE & DUISENBERG, A. J. M. (1984). *Enraf–Nonius CAD-4F Diffractometer Software Update*, February 1984. Enraf–Nonius, Groningen and Utrecht, The Netherlands.

BROWN, D. (1981). *Structure and Bonding in Crystals*, Vol. II, edited by M. O'KEEFFE & A. NAVROTSKY, pp. 1–30. New York: Academic Press.

COLAITIS, D. (1989). *J. Solid State Chem.* **83**, 158–169.

DUMAS, J., SCHLENKER, C., MARCUS, J. & BUDER, R. (1983). *Phys. Rev. Lett.* **50**, 757–760.

GANNE, M., BOUMAZA, A., DION, M. & DUMAS, J. (1985). *Mater. Res. Bull.* **20**, 1297–1308.

GHEDIRA, M., CHENAVAS, J., MAREZIO, M. & MARCUS, J. (1985). *J. Solid State Chem.* **57**, 300–313.

GOODENOUGH, J. B. (1965). *Bull. Soc. Chim. Fr.* **4**, 1200–1207.

GOODENOUGH, J. B. (1970). *J. Solid State Chem.* **1**, 349–358.

GRAHAM, J. & WADSLEY, A. D. (1966). *Acta Cryst.* B**20**, 93–100.

GRÜNER, G. (1988). *Rev. Mod. Phys.* **60**, 1129–1181.

HALL, S. R. & STEWART, J. M. (1987). Editors. *XTAL2.2 Users Manual*. Univs. of Western Australia, Australia, and Maryland, USA.

HUTIRAY, G. & SOLYOM, J. (1985). *Charge Density Waves in Solids*, Springer Lecture Notes in Physics Vol. 217, pp. 17–22, 439–448. Berlin: Springer Verlag.

JANNER, A., JANSSEN, T. & DE WOLFF, P. M. (1983). *Acta Cryst.* A**39**, 671–678.

MUMME, W. G. & WATTS, J. A. (1970). *J. Solid State Chem.* **2**, 16–23.

POUGET, J. P., NOGUERA, C., MOUDDEN, A. H. & MORET, R. (1985). *J. Phys. (Paris)*, **46**, 1731–1742.

SATO, M., FUJISHITA, H., SATO, S. & HOSHINO, S. (1985). *J. Phys. C*, **18**, 2603–2614.

SCHLENKER, C. (1989). *Low-Dimensional Electronic Properties of Molybdenum Bronzes and Oxides*, edited by C. SCHLENKER, pp. 159–252. Dordrecht: Kluwer Academic Publishers.

SCHLENKER, C. & DUMAS, J. (1986). *Crystal Chemistry and Properties of Materials with Quasi-One-Dimensional Structures*, edited by J. ROUXEL, pp. 135–177. Dordrecht: Reidel.

SCHUTTE, W. J. & DE BOER, J. L. (1988). *Acta Cryst.* B**44**, 486–494.

SCHUTTE, W. J. & DE BOER, J. L. (1993). *Acta Cryst.* B**49**. In the press.

SEGRANSAN, P., JANOSSY, A., BERTHIER, C., MARCUS, J. & BUTAUD, P. (1986). *Phys. Rev. Lett.* **56**, 1854–1857.

SMAALEN, S. VAN, BRONSEMA, K. D. & MAHY, J. (1986). *Acta Cryst.* B**42**, 43–50.

STEPHENSON, N. C. & WADSLEY, A. D. (1965). *Acta Cryst.* **19**, 241–247.

TRAVAGLINI, G. & WACHTER, P. (1983). *Solid State Commun.* **47**, 217–221.

TSAI, P. P., POTENZA, J. A. & GREENBLATT, M. (1987). *J. Solid State Chem.* **69**, 329–335.

WOLFF, P. M. DE, JANSSEN, T. & JANNER, A. (1981). *Acta Cryst.* A**37**, 625–636.

YAMAMOTO, A. (1985). *REMOS85.0. Computer Program for the Refinement of Modulated Structures*. National Institute for Research in Inorganic Materials, Sakura-Mura, Niihari-Gun, Ibaraki 305, Japan.

ZACHARIASEN, W. H. (1978). *J. Less Common Met.* **62**, 1–7.

Acta Cryst. (1993). B**49**, 591–599

Charge Densities of Two Rutile Structures: NiF_2 and CoF_2

BY M. M. R. COSTA, J. A. PAIXÃO, M. J. M. DE ALMEIDA AND L. C. R. ANDRADE

Centro FC1, INIC, Department of Physics, University of Coimbra, 3000 *Coimbra, Portugal*

(*Received* 29 *July* 1992; *accepted* 12 *February* 1993)

Abstract

X-ray diffraction data were collected at room temperature for two rutile structures, NiF_2 and CoF_2. Two different crystals of each compound have been used in the experiments. Atomic and thermal parameters were derived from least-squares refinements of high-angle data [$(\sin\theta)/\lambda \geq 0.6$ Å^{-1}]. The results of